9

Corrections to the parton model in QCD

In Ch. 8, factorization was formulated for DIS. The proofs were, however, restricted to non-gauge theory. But the results remain true in QCD, with some complications to be treated in Ch. 11.

So in this chapter we will simply assume factorization holds in QCD, and on that basis introduce methods of applying it phenomenologically. In QCD, with an unpolarized target, we will calculate: (a) the first correction terms to the hard scattering for DIS, and (b) the leading term in the kernel for DGLAP evolution of quark and gluon densities. These are the primary phenomenological tools for quantitatively analyzing DIS in QCD.

The calculations also provide an opportunity to introduce some of the complications that arise in QCD and that must be taken into account in a correct proof of factorization.

The results on which this chapter depends are: factorization for the hadronic tensor, (8.81); factorization for the structure functions (8.83); the decomposition of the partonic hard scattering tensor in terms of parton structure functions (8.82); the definition of parton densities in QCD in Sec. 7.5; the structure of their renormalization (8.11); the corresponding DGLAP evolution equations, from Sec. 8.4.

9.1 Lowest order

The parton-model calculation in (2.28) gives the first terms in the expansion of the partonic structure functions in powers of α_s:

$$\hat{F}_{1j}(Q^2, x/\xi; \alpha_s, \mu) = \frac{e_j^2}{2}\,\delta(x/\xi - 1) + O(\alpha_s), \tag{9.1a}$$

$$\hat{F}_{2j}(Q^2, x/\xi; \alpha_s, \mu) = e_j^2\,\delta(x/\xi - 1) + O(\alpha_s), \tag{9.1b}$$

and of course $\hat{F}_{jL} = 0 + O(\alpha_s)$. These are the lowest-order (LO) terms, and they apply to quarks; the gluonic coefficients start at order α_s.

9.2 Projections onto structure functions

In Feynman-graph calculations we will use projectors of a hadronic or partonic tensor onto corresponding structure functions. In the partonic case these follow simply from (8.82). It

is convenient to use the longitudinal structure function:

$$\hat{F}_{\mathrm{L}j} \stackrel{\text{def}}{=} \hat{F}_{2j} - 2\frac{x}{\xi}\hat{F}_{1j} = \frac{8(x/\xi)^3}{Q^2}\hat{k}_\mu \frac{1}{2}\operatorname{Tr} C_j^{\mu\nu}\hat{k}_\nu, \tag{9.2a}$$

$$\hat{F}_{2j} = \frac{x/\xi}{1-\epsilon}\left(-g_{\mu\nu}\frac{1}{2}\operatorname{Tr} C_j^{\mu\nu}\right) + \frac{3-2\epsilon}{2-2\epsilon}\hat{F}_{jL}, \tag{9.2b}$$

where we give the result for a general space-time dimension $4 - 2\epsilon$, as needed later. The factor $\frac{1}{2}\operatorname{Tr}$ projects onto the partonic tensor for an unpolarized parton.

9.3 Complications in QCD

9.3.1 Use of on-shell quarks and gluons

It would be possible to obtain hard-scattering coefficients and DGLAP kernels from direct use of the subtractive methods of Ch. 8. Instead we use a method where we start from calculations of structure functions and parton densities with massless quarks and gluons used as the target states.

Now starting from calculations of structure functions and parton densities on some set of target states, we can use the factorization and renormalization formulae to deduce the hard-scattering coefficient functions and the renormalization factors (of parton densities). From the renormalization factors, we deduce the DGLAP kernels. It is the coefficient functions and the DGLAP kernels that are of actual phenomenological interest, since they are perturbative.

Because these quantities are independent of the target state, we are entitled to use whatever targets are convenient for calculations. This leads us to use single on-shell quarks and gluons as the target states, with all calculations done in low-order perturbation theory. Moreover, the quantities to be calculated are independent of mass, so we also set masses to zero everywhere, since this considerably simplifies calculations of Feynman graphs.

Thus a noteworthy feature of many QCD calculations is that they use on-shell quarks and gluons as the target state. This is in striking contrast to the fact that (as far as is currently known) all true particle states in QCD are composites, i.e., bound states like the proton. Moreover there are IR and collinear divergences in perturbative calculations with on-shell massless target states. These can be regulated satisfactorily and cancel in the calculations of the coefficients, which are all short-distance dominated.

9.3.2 Choice of gauge

Another complication in QCD concerns the choice of gauge. We could use $A^+ = 0$ gauge, in which case the structure of the leading regions, for renormalization and for factorization, appears to be simplified to be the same as in a non-gauge theory (Ch. 8). However, calculations are plagued by divergences associated with the $1/k^+$ singularity in the gluon propagator. The divergences cancel, but in a non-trivial manner. This of course indicates

that extensions are needed for the proofs of factorization and renormalization that we gave in Secs. 8.3.6 and 8.9.

The alternative, which we will adopt here, is to use Feynman gauge (or a standard covariant gauge). The necessary proofs will come later. For the purposes of calculations, we simply rely on the full statement of renormalization (and factorization) applied with gauge-invariant parton densities. We will in fact still find extra divergences, characterized as rapidity divergences. We will see that the rapidity divergences cancel, non-trivially. The Feynman gauge lends itself better to good derivations of renormalization and factorization than the $A^+ = 0$ gauge.

It is interesting that there was a long-standing disagreement for calculations at two-loop order for the DGLAP kernels. This was between a calculation in light-cone gauge (Furmanski and Petronzio, 1980), and ones in Feynman gauge (Floratos, Ross, and Sachra-jda, 1979; Gonzalez-Arroyo and Lopez, 1980; Floratos, Lacaze, and Kounnas, 1981). It turned out that the light-cone gauge calculation is the correct one. The actual calculations are done with massless quarks and gluons; one has a choice between on-shell calculations and off-shell calculations. As we will see, on-shell calculations are much easier algorithmically, but suffer from various kinds of IR and collinear divergence that need to be disentangled from the UV divergences of interest. Off-shell, there are extra parton-density-like objects defined by operators other than the gauge-invariant ones needed in physical matrix elements. A subtle interaction between the IR problems and the non-gauge-invariant operators needed to be sorted out (Hamberg and van Neerven, 1992; Collins and Scalise, 1994), over a decade later than the original calculations. See Sec. 11.4 for some more details.

These problems will not affect our one-loop calculations.

9.4 One-loop renormalization calculations in QCD

In this section, we calculate the one-loop renormalization of the parton densities in QCD, starting from the definitions (7.40) and (7.43) for the bare parton densities. Then we will deduce one-loop values for the DGLAP kernels, which are phenomenologically very important in determining the evolution of parton densities with scale. The results are also essential to calculations of the hard-scattering coefficient functions.

9.4.1 General principles of calculation

Just as in our calculations in Yukawa theory, Sec. 8.7, we work with target states that are in turn a gluon or any flavor of quark. The primary new feature is that each parton density has a Wilson line, for which the Feynman rules were given in Figs. 7.10–7.12. The renormalization coefficients are adjusted so that the renormalized parton densities defined by (8.11) have no UV divergences. The general notation for the expansions in α_s was given in (8.49), and the relation between the n-loop expansion of the bare and renormalized parton densities was given in (8.52).
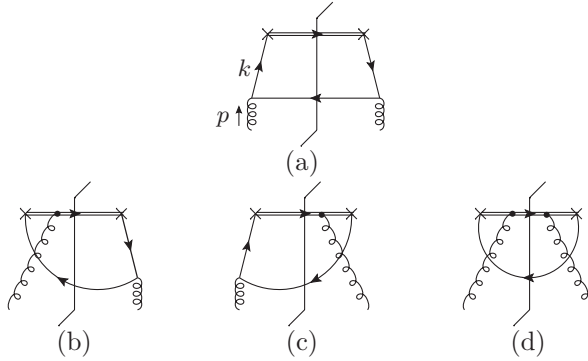
Fig. 9.1. (a) One-loop graph for renormalization of density of quark in gluon. (b)–(d) Graphs that are zero when the gluon polarization is chosen to obey $e_p^+ = 0$.

At one loop this is simple, because of the trivial zero-loop terms (8.50) and (8.51) for the renormalization and the parton densities. The factorized form for renormalization thus shows that the one-loop renormalized parton density in a quark or gluon target is the sum of the one-loop bare parton density and the one-loop renormalization coefficient:

$$f_{j/k}^{[1]}(\xi) = (Z_{2j}^{-1} f)_{(0)j/k}^{[1]}(\xi) + (Z_{2j} Z)_{jk}^{[1]}(\xi, g, \epsilon)$$

$$= (Z_{2j}^{-1} f)_{(0)j/k}^{[1]}(\xi) + Z_{2j}^{[1]} \delta_{jk} \delta(\xi - 1) + Z_{jk}^{[1]}(\xi, g, \epsilon). \tag{9.3}$$

To obtain this, we wrote the bare parton density as $Z_{2j}(Z_{2j}^{-1} f_{(0)j/k})$, where Z_{2j} is the wave function renormalization for the field for parton j. Then we separated out the one-loop terms for the Z_{2j} and for $(Z_{2j}^{-1} f_{(0)j/k})$. The reason is that $(Z_{2j}^{-1} f_{(0)j/k})$ is the parton density defined with renormalized fields instead of bare fields, so that it is a natural object to compute in perturbation theory.

We now apply the above formula to each possibility for j and k.

9.4.2 Quark in gluon

The simplest calculation is for the order g^2 off-diagonal gluon-to-quark term, i.e., in (9.3) we set k to a gluon and j to any quark flavor. The target state is a on-shell gluon with a physical polarization vector e_p^μ that has zero plus and minus components. The single graph we need is shown in Fig. 9.1(a). Since $e_p^+ = 0$, graphs (b)–(d), in which the gluon attaches to the Wilson line, are zero. [Generally the polarization vector of a on-shell gluon (or photon) of momentum p must obey $p \cdot e_p = 0$, and $e_p \cdot e_p^* = -1$. It is arbitrary up to a gauge transformation, i.e., up to the addition of a multiple of p. The choice of a gauge condition on the polarization vector may be made separately for each on-shell gluon. We have chosen the condition $e_p^+ = 0$.]

A straightforward application of the Feynman rules gives the value of the bare graph (before renormalization):

$$\frac{g^2}{16\pi^2} f_{(0),q/g}^{[1]}(\xi) = -T_F g^2 \mu^{2\epsilon} \int \frac{\mathrm{d}k^- \, \mathrm{d}^{2-2\epsilon} \boldsymbol{k}_{\mathrm{T}}}{(2\pi)^{4-2\epsilon}} \frac{2\pi \delta\left((p-k)^2 - m_q^2\right)}{(k^2 - m_q^2)^2}$$

$$\times \mathrm{Tr}\, \frac{\gamma^+}{2} (\slashed{k} + m_q)\slashed{\epsilon}_p (\slashed{k} - \slashed{p} + m_q)\slashed{\epsilon}_p^* (\slashed{k} + m_q).$$

$$= \frac{g^2 \mathrm{T}_F (4\pi\mu^2)^\epsilon}{8\pi^2 \Gamma(1-\epsilon)} \int_0^\infty \mathrm{d}k_{\mathrm{T}}^2 \frac{k_{\mathrm{T}}^{-2\epsilon}}{(k_{\mathrm{T}}^2 + m_q^2)^2}$$

$$\times \left\{ (k_{\mathrm{T}}^2 + m_q^2)\left[1 - \frac{2\xi(1-\xi)}{1-\epsilon}\right] + m_q^2 \frac{2\xi(1-\xi)}{1-\epsilon} \right\}$$

$$= \frac{g^2 T_F}{8\pi^2} \left(\frac{m_q^2}{4\pi\mu^2}\right)^{-\epsilon} \Gamma(\epsilon)\left[(1-\xi)^2 + \xi^2\right]. \tag{9.4}$$

The overall minus sign in the first line arises because of the fermion loop. For information about T_F and other group theory coefficients, see Sec. A.11. The dependence on the direction of the polarization vector has dropped out because of invariance under rotations around the z axis. Unlike the case of our later calculations we have kept a non-zero mass.

The renormalization counterterm $Z_{qg}^{[1]}$ in (9.3) is added to give a finite result at $\epsilon = 0$. In the $\overline{\mathrm{MS}}$ scheme

$$\frac{g^2}{16\pi^2} Z_{qg}^{[1]}(z) = -\frac{g^2 T_F}{8\pi^2} \frac{S_\epsilon}{\epsilon} \left[(1-z)^2 + z^2\right]. \tag{9.5}$$

From the QCD version of (8.33), the corresponding term in the DGLAP kernel is

$$\frac{g^2}{16\pi^2} P_{qg}^{[1]}(z) = \frac{g^2 T_F}{8\pi^2} \left[(1-z)^2 + z^2\right]. \tag{9.6}$$

To this order the finite renormalized density of a quark in a gluon is

$$\frac{g^2}{16\pi^2} f_{q/g}^{[1]}(\xi) = \frac{g^2 T_F}{8\pi^2} \left[(1-\xi)^2 + \xi^2\right] \ln \frac{\mu^2}{m_q^2}. \tag{9.7}$$

This calculation, with its non-zero quark mass, will appear as a subtraction component in calculations of hard-scattering coefficients for heavy quark production. But the $\overline{\mathrm{MS}}$ renormalization coefficient is independent of mass, so its calculation can equally well be performed with a zero quark mass. Moreover hard-scattering calculations, which we will examine later, are considerably simplified when masses are neglected with respect to the hard scale Q. So we now examine what happens when we set $m_q = 0$. The bare graph's integral is now

$$\frac{g^2 \mathrm{T}_F (4\pi\mu^2)^\epsilon}{8\pi^2 \Gamma(1-\epsilon)} \int_0^\infty \mathrm{d}k_{\mathrm{T}}^2 \frac{k_{\mathrm{T}}^{-2\epsilon}}{k_{\mathrm{T}}^2} \left[1 - \frac{2\xi(1-\xi)}{1-\epsilon}\right]. \tag{9.8}$$
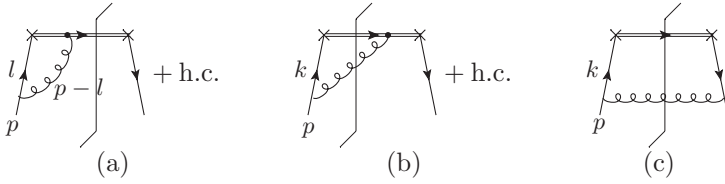
Fig. 9.2. One-loop graphs for renormalization of density of quark in quark. Hermitian conjugates of (a) and (b) should be added. As explained in the text, graphs with a quark self-energy graph need not be considered explicitly, and graphs where the gluon connects the Wilson line to itself are zero.

The integral is of a simple power of k_T, which is elementary compared to (9.4), with its beta function. However, the integral has an extra divergence at $k_T = 0$. This is a collinear divergence, since it happens when the quark and antiquark are parallel to the gluon. Dimensional regularization regulates both the UV and the collinear divergence, but only by going in opposite directions in ϵ. Even so, such integrals can be consistently defined (e.g., Collins, 1984, Ch. 4) and it is a theorem that integrals of a power of the integration variable are zero in dimensional regularization. Thus the collinear and UV divergences are equal and opposite. The UV pole can be obtained by examining the part of the integral in (9.8) from a non-zero value of k_T to infinity. Then the renormalized value of the graph is the negative of the UV pole:

$$\frac{g^2}{16\pi^2} f_{q/g}^{[1]}(\xi; m=0) = \frac{g^2}{16\pi^2} f_{(0)q/g}^{[1]}(\xi; m=0) + \frac{g^2}{16\pi^2} Z_{qg}^{[1]}(z)$$

$$= 0 - \frac{g^2 T_F}{8\pi^2} \frac{S_\epsilon}{\epsilon} \left[(1-\xi)^2 + \xi^2 \right]. \tag{9.9}$$

That the renormalized value is collinear divergent reflects the masslessness of both the quark and the gluon, and that the asymptotic scattering states do not obey the standard rules. Of course, neither the massless limit (for quarks) nor the existence of an isolated gluon (or quark) is a feature of real QCD. As already stated, such massless calculations are useful as components of calculations of hard-scattering coefficients, for which the massless limit does exist, as we will verify explicitly. Thus the existence of a collinear (or other kind of IR) divergence in a renormalized partonic matrix element is not a fundamental problem.

9.4.3 Quark in quark

We next apply the same principles to the density of a quark in a quark, for which the one-loop graphs are shown in Fig. 9.2, with virtual gluon emission in graph (a) and real gluon emission in graphs (b) and (c). There is, in principle, a term where both ends of the gluon attach to the Wilson line. But as we will review below, this term is effectively zero.

We do not include a self-energy correction for the incoming quark, since its renormalization is done by a counterterm in the Lagrangian. Indirectly its effects will appear, in the renormalization factor of the parton density, because of the Z_2 term in (9.3).

Gluon polarization sum

In the graphs with real gluon emission, we use a physical gluonic final state, so that the sum over gluon polarizations, is a sum over physical (transverse) polarizations for the gluon. However, very generally, the sum over physical final states can be extended to a sum over all final states (including when necessary ghost-antighost pairs, which will not concern us here). This is shown in field theory textbooks (e.g., Ch. 11 of Sterman, 1993) under the heading of "Unitarity of the S-matrix". Thus we may replace the sum over transverse gluon polarizations in Figs. 9.2(b) and (c) by the same numerator $-g^{\alpha\beta}$ that appears in the Feynman-gauge gluon propagator. Since $g^{++} = 0$, graphs where both ends of the gluon attach to the Wilson line are zero, so we omit these graphs.

The proof at the level of the emission of one gluon of momentum l goes as follows. Representatives of physical polarizations obey $l \cdot e = 0$, and it is easy to check that the polarization sum obeys

$$\sum_{\text{phys pols.}} e^{\alpha}(e^{\beta})^* = -g^{\alpha\beta} + l^{\alpha}b^{\beta} + b^{\alpha}l^{\beta} = -g^{\alpha\beta} + \text{terms giving zero by WI}, \quad (9.10)$$

where b is some vector. The terms with a factor l give zero by a Ward identity, after a sum over graphs.

Virtual correction

The virtual gluon correction in Fig. 9.2(a) (*with its hermitian conjugate*) gives

$$\frac{g^2}{16\pi^2} f_{(0),q/q}^{(a+a^\dagger)}(\xi) = 2\delta(p^+ - \xi p^+)\frac{-ig^2 C_F \mu^{2\epsilon}}{(2\pi)^{4-2\epsilon}}$$

$$\times \int d^{4-2\epsilon}l \frac{\text{Tr}\,\frac{\gamma^+}{2}\slashed{l}\gamma^+\frac{\slashed{p}}{2}}{(l^2+i0)[(p-l)^2+i0](-p^+ + l^+ + i0)}$$

$$= -\delta(1-\xi)\frac{g^2 C_F(4\pi\mu^2)^\epsilon}{4\pi^2\Gamma(1-\epsilon)}\int_0^1 d\alpha \frac{\alpha}{1-\alpha}\int_0^\infty dl_{\text{T}}^2 \frac{l_{\text{T}}^{-2\epsilon}}{l_{\text{T}}^2}, \quad (9.11)$$

where $\alpha = l^+/p^+$. The missing steps are to express the integral in light-front coordinates, and then to perform the l^- integral by contour methods. We have chosen to do the calculation with all masses set to zero. As before, the transverse-momentum integral is of the scale-free kind that gives zero. The negative of the UV divergence gives the graph's contribution to the renormalization:

$$\frac{g^2}{16\pi^2}(Z_2 Z)_{qq}^{(a+a^\dagger)}(z, g, \epsilon) = \frac{g^2 C_F S_\epsilon}{4\pi^2\epsilon}\,\delta(1-z)\int_0^1 d\alpha \frac{\alpha}{1-\alpha}. \quad (9.12)$$

Notice that we have now explicitly needed to show the factor of Z_2 in the renormalization factor.

An important new feature is that there is an *un*regulated divergence in the integral over α at $\alpha = 1$. We will see that the divergence cancels against a similar divergence in graph (b), but it is first worth examining the source of the divergence. There are multiple sources

of divergence in the integral in the last line of (9.11), and they each have a different status for our ultimate phenomenological uses of the results of our calculations. So we need to make their nature apparent. We first insert non-zero quark and gluon masses, m_q and m_g, in the calculation to regulate with the IR problems. It is readily checked that the effect is to replace the $1/l_T^2$ factor in (9.11) by

$$\frac{1}{l_T^2 + m_g^2\alpha + m_q^2(1-\alpha)^2}. \tag{9.13}$$

Now, when the gauge symmetry is non-abelian, as in QCD, a non-zero gluon mass is not allowed. However, to understand the divergences we temporarily consider the same calculation in an abelian theory, where a non-zero gauge boson mass can be used.

With the non-zero masses, there is no longer a divergence at $l_T = 0$, but we still have a divergence at $\alpha \to 1$. Relative to the simpler parton densities which we calculated earlier, the $1/(1-\alpha)$ singularity arises from the Wilson-line denominator. After a contour deformation, the divergence occurs when the $(+, -, T)$ components of the gluon momentum are of order $((1-\alpha)p^+, l_T^2/((1-\alpha)p^+), l_T)$, for fixed l_T. The rapidity of the gluon goes to $-\infty$; the gluon can in fact be regarded as collinear to the Wilson line, which has rapidity $y = \frac{1}{2}\ln(n^+/n^-) = -\infty$. The quark goes far off-shell here.

So we call the divergence at $\alpha = 1$ a rapidity divergence. The region evidently has nothing to do with the parton-model physics that a parton density is supposed to capture. When we investigate transverse-momentum-dependent parton densities, we will need to use a Wilson line with a finite rapidity to get an appropriate definition with no rapidity divergence. But for an integrated density we will see a cancellation.

Notice from the denominator in (9.13) that if the gluon mass is zero, there is in addition a divergence at $l_T = 0$ and $\alpha = 1$. This is just like the IR divergence in QED. Finally, if also the quark mass is zero, there is also a divergence when the gluon is collinear to the initial state (at $l_T = 0$ and $\alpha \neq 0, 1$).

Real correction, first part

Figure 9.2(b) plus its hermitian conjugate give

$$\frac{g^2}{16\pi^2} f_{(0),q/q}^{(b+b^\dagger)}(\xi) = 2\frac{-g^2 C_F \mu^{2\epsilon}}{(2\pi)^{4-2\epsilon}} \int d^{2-2\epsilon} \boldsymbol{k}_T \, dk^- \, 2\pi\delta((p-k)^2)\frac{\text{Tr}\,\frac{\gamma^+}{2}\slashed{k}\gamma^+\frac{\slashed{p}}{2}}{k^2(p^+-k^+)}$$

$$= \frac{g^2 C_F(4\pi\mu^2)^\epsilon}{4\pi^2\Gamma(1-\epsilon)}\frac{\xi}{1-\xi}\int_0^\infty dk_T^2 \frac{k_T^{-2\epsilon}}{k_T^2}, \tag{9.14}$$

The minus sign in the first line arises from the gluon numerator, which is $-g^{\alpha\beta}$ in accordance with the discussion around (9.10). Notice that this formula is almost the same as the integrand for the virtual correction, which comes from a graph related by moving the final-state cut. In fact, we can get the virtual term from the above formula by: (1) changing ξ to α and integrating over it; (2) changing the label of the transverse momentum; (3) inserting a delta function; (4) reversing the sign. If we integrated over ξ (from 0 to 1 of course), there would be a perfect cancellation.

The corresponding contribution to the renormalization is

$$\frac{g^2}{16\pi^2} Z_{qq}^{(b+b^\dagger)}(z, g, \epsilon) = -\frac{g^2 C_F S_\epsilon}{4\pi^2 \epsilon} \frac{z}{1-z}. \tag{9.15}$$

9.4.4 Cancellation of divergence: the plus distribution

All of the quantities involved – parton densities, renormalization factors, DGLAP kernels – have rapidity divergences in individual graphs. For a systematic treatment, we must regard all of these quantities not as ordinary functions, but as a generalized functions. That is, they only have numerical values when integrated with a smooth test function. After this, we will see a cancellation of the rapidity divergences.

So we integrate the sum of graphs (a) and (b) (plus conjugates) with a smooth function $T(\xi)$, to obtain

$$\frac{g^2}{16\pi^2} f_{(0),q/q}^{(a+b+h.c.)}[T] \overset{\text{def}}{=} \frac{g^2}{16\pi^2} \int d\xi \, f_{(0),q/q}^{(a+b+h.c.)}(\xi) \, T(\xi)$$

$$= \frac{g^2 C_F (4\pi\mu^2)^\epsilon}{4\pi^2 \Gamma(1-\epsilon)} \int_0^1 d\xi \, \frac{\xi[T(\xi) - T(1)]}{1-\xi} \int_0^\infty dk_T^2 \, \frac{k_T^{-2\epsilon}}{k_T^2}. \tag{9.16}$$

To obtain the contribution from the virtual graph, we used the $\delta(\xi - 1)$ factor to perform the ξ integral, and then changed the name of the variable α to ξ. The divergence at $\xi \to 1$ has now canceled.

To express these graphs directly in ξ space, it is convenient to define the so-called plus distribution:

$$\int_0^1 dx \left(\frac{1}{1-x}\right)_+ T(x) \overset{\text{def}}{=} \int_0^1 dx \, \frac{T(x) - T(1)}{1-x}. \tag{9.17}$$

We will often meet this distribution multiplied by polynomials in ξ, in which case we will put the + subscript on the denominator:

$$\int_0^1 dx \, \frac{A(x)}{(1-x)_+} T(x) \overset{\text{def}}{=} \int_0^1 dx \, \frac{A(x)T(x) - A(1)T(1)}{1-x}. \tag{9.18}$$

Then the combination we need in the sum of graphs is

$$\int_0^1 d\xi \, \frac{[T(\xi) - T(1)]\xi}{1-\xi} = \int_0^1 d\xi \left[\frac{\xi T(\xi) - T(1)}{1-\xi} + T(1)\right]$$

$$= \int_0^{1+} d\xi \left[\frac{\xi}{(1-\xi)_+} + \delta(\xi - 1)\right] T(\xi), \tag{9.19}$$

so that the sum of graphs (a) and (b) is

$$\frac{g^2}{16\pi^2} f_{(0),q/q}^{(a+b+h.c.)}(\xi) = \frac{g^2 C_F (4\pi\mu^2)^\epsilon}{4\pi^2 \Gamma(1-\epsilon)} \left[\frac{\xi}{(1-\xi)_+} + \delta(\xi - 1)\right] \int_0^\infty dk_T^2 \, \frac{k_T^{-2\epsilon}}{k_T^2}. \tag{9.20}$$

Real correction, second part

Figure 9.2(c) gives no such complications. Its value is

$$
\frac{g^2}{16\pi^2} f_{(0),q/q}^{(c)}(\xi) = \frac{-g^2 C_F \mu^{2\epsilon}}{(2\pi)^{4-2\epsilon}} \int d^{2-2\epsilon} \boldsymbol{k}_{\mathrm{T}}\, dk^- \, 2\pi \delta((p-k)^2) \frac{\mathrm{Tr}\, \frac{\gamma^+}{2}\slashed{k}\gamma^\mu \frac{\slashed{p}}{2}\gamma_\mu \slashed{k}}{(k^2)^2}
$$

$$
= \frac{g^2 C_F (4\pi\mu^2)^\epsilon}{8\pi^2 \Gamma(1-\epsilon)} (1-\xi)(1-\epsilon) \int_0^\infty dk_{\mathrm{T}}^2 \frac{k_{\mathrm{T}}^{-2\epsilon}}{k_{\mathrm{T}}^2}. \tag{9.21}
$$

Total one-loop value for renormalization and DGLAP kernel

We can now combine the UV divergences from the various graphs with the Z_2 term in (9.3), whose value is in (3.23). Then the one-loop renormalization of the quark density is

$$
\frac{g^2}{16\pi^2} Z_{jk}^{[1]}(z; \mathrm{quark}) = -\frac{g^2 C_F \delta_{jk}}{8\pi^2} \frac{S_\epsilon}{\epsilon} \left[\frac{1+z^2}{(1-z)_+} + \frac{3}{2}\delta(z-1) \right]. \tag{9.22}
$$

From (8.31) and (8.33), the resulting DGLAP kernel is

$$
\frac{g^2}{16\pi^2} P_{jk}^{[1]}(z; \mathrm{quark}) = \frac{g^2 C_F \delta_{jk}}{8\pi^2} \left[\frac{1+z^2}{(1-z)_+} + \frac{3}{2}\delta(z-1) \right]
$$

$$
= \frac{g^2 C_F \delta_{jk}}{8\pi^2} \left[\frac{2}{(1-z)_+} - 1 - z + \frac{3}{2}\delta(z-1) \right]. \tag{9.23}
$$

9.4.5 Gluon-in-gluon and gluon-in-quark

Similar calculations can be done for the case of a gluon in a gluon, and for a gluon in a quark. The actual calculations we leave as an exercise, with the results being (Altarelli and Parisi, 1977)

$$
\frac{g^2}{16\pi^2} P_{gg}^{[1]}(z) = \frac{g^2}{8\pi^2} \left\{ 2C_A \left[\frac{z}{(1-z)_+} + \frac{1-z}{z} + z(1-z) \right] + \delta(z-1)\frac{11C_A - 4n_f T_R}{6} \right\}, \tag{9.24}
$$

$$
\frac{g^2}{16\pi^2} P_{gq}^{[1]}(z) = \frac{g^2 C_F}{8\pi^2} \left[\frac{1+(1-z)^2}{z} \right]. \tag{9.25}
$$

9.5 One-loop renormalization by subtraction of asymptote

We saw in Sec. 3.4 that UV renormalization, at least at one-loop order, could be implemented by subtraction of the asymptotic large transverse-momentum asymptote of a Feynman graph. This enabled us to give a strictly four-dimensional interpretation of minimal subtraction.

In this section we show how to apply this method to the renormalization of parton densities. This will serve two aims. One is to show how to make a physically appropriate choice of the renormalization scale μ. The second aim concerns calculations of hard-scattering coefficients, which normally employ massless quarks and gluons. At intermediate stages of the calculations, collinear and soft divergences appear, which cancel in the final result. Generally dimensional regularization is used to regulate the divergences, but it is useful to show how to work with a purely four-dimensional integral. One virtue of this method is to allow the immediate use of the compendium of purely four-dimensional amplitudes in Gastmans and Wu (1990).

It is important that our results have extra finite counterterms compared with the illustrative example in Sec. 3.4.

9.5.1 Quark in gluon

The unsubtracted one-loop integral for the density of a quark in a gluon is (9.4). The renormalized value is given by adding an $\overline{\text{MS}}$ counterterm, obtained from the renormalization term (9.5) by substituting $z \mapsto \xi$. We write the counterterm as the integral over the asymptote of the original integrand plus a finite correction $R_{q/g}$, to be determined:

$$
-\frac{g^2 T_F}{8\pi^2} \frac{S_\epsilon}{\epsilon} [1 - 2(1-\xi)\xi]
$$
$$
= -\frac{(4\pi\mu^2)^\epsilon}{\Gamma(1-\epsilon)} \frac{g^2 T_F}{8\pi^2} \int_{\mu^2}^\infty \frac{dk_T^2}{(k_T^2)^{1+\epsilon}} \left[1 - \frac{2(1-\xi)\xi}{1-\epsilon} \right] + R_{q/g}
$$
$$
= -\frac{g^2 T_F}{8\pi^2} \frac{(4\pi)^\epsilon}{\epsilon\,\Gamma(1-\epsilon)} \left[1 - \frac{2(1-\xi)\xi}{1-\epsilon} \right] + R_{q/g}, \qquad (9.26)
$$

where S_ϵ is given in (A.41). Hence

$$
R_{q/g} = -\frac{g^2 T_F}{8\pi^2} \frac{S_\epsilon}{1-\epsilon} 2(1-\xi)\xi \overset{\epsilon \to 0}{\to} -\frac{g^2 T_F}{8\pi^2} 2(1-\xi)\xi. \qquad (9.27)
$$

Only the value of $R_{q/g}$ at $\epsilon = 0$ is needed in a purely four-dimensional formula.

With this method the renormalized density at $\epsilon = 0$ is

$$
\frac{g^2}{16\pi^2} f_{q/g}^{[1]}(\xi) = \frac{g^2 T_F}{8\pi^2} \left\{ \int_0^\infty dk_T^2 \left[\frac{1 - 2\xi(1-\xi)}{k_T^2 + m_q^2} + \frac{m_q^2 2\xi(1-\xi)}{(k_T^2 + m_q^2)^2} \right.\right.
$$
$$
\left.\left. - \theta(k_T - \mu) \frac{1 - 2\xi(1-\xi)}{k_T^2} \right] - 2(1-\xi)\xi \right\}. \quad (9.28)
$$

It can be checked that this is the same as the previously calculated value (9.7), but the integrals are algorithmically simpler, because they do not involve the beta functions that arise with the dimensionally regulated integrals. Because of the extra term $2(1-\xi)\xi$, it cannot be literally said that the integrated parton density is the integral of the unintegrated density with a cutoff at $k_T = \mu$, even for large μ. This is contrary to statements that appear in the literature (e.g., Watt, Martin, and Ryskin, 2003).

9.5.2 Other cases

The remaining cases are left as an exercise (problem 9.3) with the results:

$$R_{g/q}(\epsilon = 0) = -\frac{g^2 C_F}{8\pi^2}\, 4\xi, \tag{9.29}$$

$$R_{q/q}(\epsilon = 0) = -\frac{g^2 C_F}{8\pi^2}\, 4(1 - \xi), \tag{9.30}$$

$$R_{g/g}(\epsilon = 0) = 0. \tag{9.31}$$

9.6 DIS on partonic target

To calculate the hard-scattering coefficients for DIS, we observe that the factorization theorem applies to any target state, while the coefficient functions $C^{\mu\nu}$ are target independent. Therefore we apply the factorization theorem in perturbation theory with targets that are on-shell quark or gluon states. Computing both the structure functions and the parton densities on partonic targets up to some order in perturbation theory enables us to deduce the hard-scattering coefficients to the same order. Moreover, since the coefficient functions are independent of masses, we will set masses to zero everywhere.

We organize perturbation expansions as we did for the renormalization of parton densities in Sec. 8.7.3. Define $W_j^{\mu\nu}$ to be the hadronic tensor for DIS with a massless on-shell partonic target of flavor j. We write perturbation expansions of $W_j^{\mu\nu}$ and $C_j^{\mu\nu}$ as

$$W_j^{\mu\nu}(x, Q) = \sum_{n=0}^{\infty} \left(\frac{g^2}{16\pi^2}\right)^n W_j^{[n],\,\mu\nu}(x, Q), \tag{9.32a}$$

$$C_j^{\mu\nu}(x, Q) = \sum_{n=0}^{\infty} \left(\frac{g^2}{16\pi^2}\right)^n C_j^{[n],\,\mu\nu}(x, Q). \tag{9.32b}$$

The nth order term in the factorization theorem (8.81) is

$$W_j^{[n],\mu\nu}(x, Q) = \sum_{n'=0}^{n} \sum_{j'} \int_{x-}^{1+} \frac{d\xi}{\xi} C_{j'}^{[n'],\mu\nu}(x/\xi, Q) \otimes f_{j'/j}^{[n-n']}(\xi). \tag{9.33}$$

Since masses are set to zero, the power-suppressed corrections in (8.81) are not present. Throughout our calculations we will work with the unpolarized case, so the partonic density matrix ρ is dropped.

We deduce a formula for the nth order hard-scattering coefficient:

$$C_j^{[n],\mu\nu}(z, Q) = W_j^{[n],\mu\nu}(z, Q) - \sum_{n'=0}^{n-1} \sum_{j'} \int_{z-}^{1+} \frac{d\zeta}{\zeta} C_{j'}^{[n'],\mu\nu}(z/\zeta, Q) f_{j'/j}^{[n-n']}(\zeta). \tag{9.34}$$

Here, to avoid confusion with symbols used when the coefficient function is substituted in the factorization formula (8.81) for a hadronic target, the names of partonic variables were changed to z and ζ. In the factorization formula, z would be replaced by x/ξ.
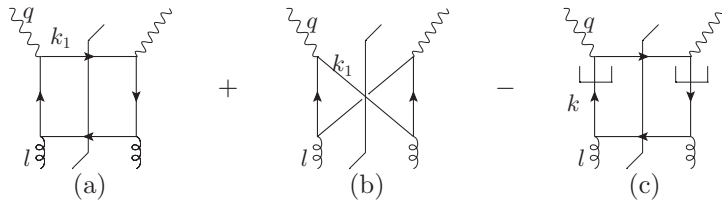
Fig. 9.3. Graphs for NLO gluon coefficient function for DIS. There are, in addition, three other graphs with the direction of the arrow on the quark loop reversed. The hooks on the quark lines in the subtraction graph (c) indicate where a parton-model approximation is made.

Equation (9.34) provides an effective recursive procedure for calculating the nth order term in C starting from the case $n = 0$, for which the result was given in (2.28), with corresponding structure functions in (9.1). At next-to-leading order (NLO) we have

$$C_j^{[1],\mu\nu}(z, Q) = W_j^{[1],\mu\nu}(z, Q) - \sum_{j'} \int_{z-}^{1+} \frac{d\zeta}{\zeta} C_{j'}^{[0],\mu\nu}(z/\zeta, Q) f_{j'/j}^{[1]}(\zeta). \tag{9.35}$$

Our calculations in Sec. 9.4 of renormalized one-loop parton densities gave the values of $f_{j'/j}^{[1]}(\zeta)$.

Perturbation theory for W and f in massless QCD suffers from IR and collinear divergences. So the radius of convergence[1] in g for these quantities goes to zero as the IR regulator ϵ goes to zero. But this is sufficient to obtain the perturbation expansion of the hard-scattering coefficients C. Since divergences cancel in the coefficient functions, their radius of convergence remains non-zero as $\epsilon \to 0$.

9.7 Computation of NLO gluon coefficient function

Applied to the NLO gluon coefficient, (9.35) requires us to compute the graphs of Fig. 9.3. The external gluons are massless and on-shell, with zero transverse momentum, and the internal quarks are massless and have a sum over flavors. Figure 9.3(c) implements the subtraction in (9.35), and we will call it a double-counting-subtraction graph, since it cancels the contribution in the first two graphs that is taken into account in the lowest-order parton model.

9.7.1 Kinematics

Let k_1 and k_2 be the momenta of the final-state quark and antiquark, and let l be the momentum $(l^+, 0, \mathbf{0}_T)$ of the gluon, so that $k_2 = q + l - k_1$. The scalar kinematic variables

---

[1] Strictly speaking, perturbation series are expected to be asymptotic series but not convergent, so the term "radius of convergence" should be replaced by some better terminology concerning the region of coupling where perturbation theory has some chosen accuracy.

relevant to the problem are Q and

$$z = \frac{Q^2}{2l \cdot q} = \frac{-q^+}{l^+}, \tag{9.36a}$$

$$\hat{s} = (k_1 + k_2)^2 = \frac{Q^2(1-z)}{z}, \tag{9.36b}$$

$$\hat{t} = (l - k_2)^2 = -\frac{Q^2(1 + \cos\theta)}{2z}, \tag{9.36c}$$

$$\hat{u} = (l - k_1)^2 = -\frac{Q^2(1 - \cos\theta)}{2z}, \tag{9.36d}$$

where θ is the scattering angle in the photon-gluon center of mass. Of these variables, only three are independent, of course.

9.7.2 Calculation of unsubtracted graphs

Graph (a) of Fig. 9.3 gives

$$-\sum_j \frac{g^2 e_j^2 T_F}{32\pi^2} \left(\frac{16\pi^2\mu^2}{\hat{s}}\right)^\epsilon \int \frac{\mathrm{d}\Omega}{4\pi} \frac{\mathrm{Tr}\, \slashed{k}_1 \gamma^\nu (\slashed{l} - \slashed{k}_2)\slashed{e}(-\slashed{k}_2)\slashed{e}^*(\slashed{l} - \slashed{k}_2)\gamma^\mu}{\left[(l - k_2)^2\right]^2}, \tag{9.37}$$

where $\mathrm{d}\Omega$ represents the integration over the angle of the quarks in the photon-gluon center of mass, and e^μ is the (transverse) polarization vector of the gluon. The overall minus sign is for a fermion loop, and the normalization arises from the $1/(4\pi)$ in the definition of $W^{\mu\nu}$, and from two-body phase space (A.43). We choose the sum over j to be *over flavors of quark only (not over antiquarks)*. Then we must add, to this and the terms for the other graphs, the contribution with the quark line reversed; this is obtained simply by exchanging k_1 and k_2.

Similarly graph (b) gives

$$-\sum_j \frac{g^2 e_j^2 T_F}{32\pi^2} \left(\frac{16\pi^2\mu^2}{\hat{s}}\right)^\epsilon \int \frac{\mathrm{d}\Omega}{4\pi} \frac{\mathrm{Tr}\, \slashed{k}_1 \gamma^\nu (\slashed{l} - \slashed{k}_2)\slashed{e}(-\slashed{k}_2)\gamma^\mu(\slashed{k}_1 - \slashed{l})\slashed{e}^*}{(l - k_2)^2 (l - k_1)^2}. \tag{9.38}$$

We are only treating unpolarized processes, so we average over gluon polarizations:

$$\frac{1}{2 - 2\epsilon} \sum e^i (e^j)^* = \frac{\delta^{ij}}{2 - 2\epsilon}, \tag{9.39}$$

with a Kronecker delta in the transverse dimensions. Then we use standard Dirac algebra, and use (9.2) to project the sum of the terms for the two graphs onto the tensor structures for $\hat{F}_{Lg}$ and $\hat{F}_{2g}$. The integrands are now independent of the azimuthal direction of the quark momenta, so we use (A.36) and (A.37) to give

$$\hat{F}_{Lg} = \sum_j \frac{g^2 e_j^2 T_F}{4\pi^2} \left(\frac{16\pi\mu^2 z}{Q^2(1-z)}\right)^\epsilon \frac{2z^2(1-z)}{(1-\epsilon)\Gamma(1-\epsilon)} \int_{-1}^1 \mathrm{d}\cos\theta \ (\sin\theta)^{-2\epsilon}$$

$$\xrightarrow{\epsilon \to 0} \sum_j \frac{g^2 e_j^2 T_F}{4\pi^2} 4z^2(1-z), \tag{9.40}$$

$$\hat{F}_{2g} = \sum_j \frac{g^2 e_j^2 T_F}{4\pi^2} \left(\frac{16\pi \mu^2 z}{Q^2(1-z)} \right)^\epsilon \frac{z}{\Gamma(1-\epsilon)} \int_{-1}^1 d\cos\theta \ (\sin\theta)^{-2\epsilon}$$

$$\times \left\{ \frac{1}{\sin^2\theta} \left[1 - \frac{2z(1-z)}{1-\epsilon} \right] + \frac{-2+5\epsilon}{4(1-\epsilon)^2} + \frac{3-2\epsilon}{(1-\epsilon)^2} z(1-z) \right\}$$

$$- \text{term from graph (c)}, \tag{9.41}$$

up to higher-order corrections ($O(g^4)$). In $\hat{F}_{Lg}$, we have omitted the subtraction from graph (c), since that involves the lowest-order parton-model hard scattering, for which there is no contribution to F_L, with fermion quarks.

9.7.3 Double-counting-subtraction graph

The subtraction graph (c) is obtained from the rules for the quark density and the LO hard scattering, which contributes only to F_2. Using the integral from (9.4) at $m_q = 0$, we get

$$\hat{F}_{2g}(\text{graph (c)}) = -\sum_j \frac{g^2 e_j^2 T_F}{4\pi^2} \frac{(4\pi\mu^2)^\epsilon z}{\Gamma(1-\epsilon)} \int_0^\infty dk_T^2 \frac{k_T^{-2\epsilon}}{k_T^2} \left[1 - \frac{2z(1-z)}{1-\epsilon} \right]$$

$$+ \sum_j \frac{g^2 e_j^2 T_F S_\epsilon z}{4\pi^2 \epsilon} [1 - 2z(1-z)], \tag{9.42}$$

where the second line is the $\overline{\text{MS}}$ counterterm for the UV divergence. As announced earlier, both of (9.41) and (9.42) are collinear divergent, at $\theta = 0$ and $\theta = \pi$, and at $k_T = 0$. Dimensional regularization with ϵ *negative* regulates the divergence. By making the change of variable $k_T^2 = (\hat{s}/4)\sin^2\theta$, we can see that the collinear singularities in the integrands are equal and opposite, and that the cancellation includes the explicit ϵ dependence. The cancellation is guaranteed by the construction of the subtraction term (c) to cancel the collinear contribution in the other graphs, to prevent double counting with the parton-model term. [When checking the cancellation, note that two values of θ correspond to a single value of k_T. Note also that the maximum value of k_T^2 for graphs (a) and (b) is $\hat{s}/4$, whereas the integral for graph (c) extends to $k_T = \infty$.]

9.7.4 Total

The $\cos\theta$ integral in (9.41) gives a beta function, with a pole at $\epsilon = 0$ caused by the collinear divergence. The k_T integral in (9.42) gives zero, leaving the UV counterterm. So we get the NLO gluonic coefficient function

$$\hat{F}_{2g}(Q^2, x/\xi; \alpha_s, \mu)$$

$$\overset{\epsilon=0}{=} \sum_j \frac{g^2 T_F e_j^2}{4\pi^2} z \left\{ [(1-z)^2 + z^2] \ln\left[\frac{Q^2(1-z)}{\mu^2 z} \right] - 1 + 8z(1-z) \right\} + O(g^4). \tag{9.43}$$

There is a somewhat complicated pattern of divergences at $\epsilon = 0$, which can be summarized as follows:

Graph	Collinear	UV	total
(a)	−1	0	−1
(b)	0	0	0
(c) graph	+1	−1	0
(c) counterterm	0	+1	+1

where the coefficients apply to the factor $\sum_j [1 - 2z(1 - z)] \, g^2 T_F e_j^2/(4\pi^2\epsilon)$. Since the transverse momentum integral in the subtraction term is exactly zero, it could be said that the $\overline{\text{MS}}$ counterterm cancels the collinear divergence. It is, in fact, a common misconception that this represents the true state of affairs. However, it is also profoundly misleading.

For example, suppose one retained the quark mass in the calculation, as might be appropriate for a quark of large mass. Then the collinear region would no longer give an actual divergence. Instead, graph (a) would be finite, but with a logarithmic enhancement from the region of small transverse momentum. Graph (c) (without its counterterm) would now be non-zero, with a UV divergence. The counterterm cancels the UV divergence. For the dominant part of the collinear contributions (that give divergences at $m_q = 0$) there is a cancellation between graphs (a) and (c). The collinear cancellation is guaranteed by the nature of the subtraction term: (c) is to prevent double counting of the parton-model contribution.

9.7.5 Use of subtraction of asymptote for UV divergence

We can also use the method of subtraction of the asymptote for the renormalization of the UV divergence, from Sec. 9.5. This gives

$$
\hat{F}_{2g}(\text{NLO}) \stackrel{?}{=} \sum_j \frac{g^2 T_F e_j^2}{4\pi^2} z \int_{-1}^{1} d\cos\theta \left[\frac{1 - 2z + 2z^2}{\sin^2\theta} - \frac{1}{2} + 3z(1 - z) \right]
$$

$$
+ \sum_j \frac{g^2 T_F e_j^2}{4\pi^2} z \left[2z(1 - z) - \int_0^{\mu^2} \frac{dk_{\mathrm{T}}^2}{k_{\mathrm{T}}^2}(1 - 2z + 2z^2) \right], \qquad (9.44)
$$

where the $2z(1 - z)$ on the second line is from $R_{q/g}(z)$ in (9.27). Each integral is separately divergent, hence the query on the equality sign. To make the integrals correspond, we convert them to use a common variable $k_T^2 = (\hat{s}/4)\sin^2\theta$. Then

$$
\hat{F}_{2g}(\text{NLO}) = \sum_j \frac{g^2 T_F e_j^2}{4\pi^2} z \left\{ (1 - 2z + 2z^2) \int_0^\infty \frac{dk_{\mathrm{T}}^2}{k_{\mathrm{T}}^2} \left[\frac{\theta(k_{\mathrm{T,max}}^2 - k_{\mathrm{T}}^2)}{\sqrt{1 - k_{\mathrm{T}}^2/k_{\mathrm{T,max}}^2}} - \theta(\mu^2 - k_{\mathrm{T}}^2) \right] \right.
$$

$$
\left. - 1 + 8z(1 - z) \right\}, \qquad (9.45)
$$

where $k_{\mathrm{T,max}}^2 = Q^2(1 - z)/(4z)$. It can be checked that this agrees with the previous result, (9.43). The advantage of this integral is that it is a fundamentally an integral in the physical space-time dimension. It also enables us to gauge the general order of magnitude of the coefficient.

9.8 Choice of renormalization scale μ

It is necessary to choose the renormalization scale μ when applying a factorization theorem. As can be seen from an example calculation, e.g., (9.43), hard-scattering coefficients depend logarithmically on Q/μ. The general situation follows from the DGLAP equation for the μ dependence of parton densities. Since structure functions are RG invariant, the hard-scattering coefficients obey an inverse DGLAP equation. It follows that at order α_s^n the hard-scattering coefficients have dependence on $\ln(Q/\mu)$ that is polynomial with a highest term $\ln^n(Q/\mu)$.

The effective expansion parameter of the hard scattering is therefore $\alpha_s(\mu) \ln(Q/\mu)$, and to make optimal use of perturbative calculations one should choose μ of order Q. Then the expansion parameter is $\alpha_s(Q)$.

However, we need more precise information about an appropriate value for the ratio μ/Q. To see that this is a non-trivial problem, consider a change of scheme for renormalizing QCD and the parton densities. A concrete example is to replace S_ϵ in the $\overline{\mathrm{MS}}$ scheme by $S_\epsilon e^{2c\epsilon}$ for some constant c. Call this the c scheme. It is related to the $\overline{\mathrm{MS}}$ scheme by a simple substitution: $\mu_{\overline{\mathrm{MS}}} = \mu_c e^c$, so that $\ln(\mu_{\overline{\mathrm{MS}}}/Q) = \ln(\mu_c/Q) + c$. Then if we set $\mu_c = Q$, the coefficients of the perturbative expansion are made arbitrarily large simply by making c large.

Evidently we can remove these large coefficients by setting μ_c to a suitable factor times Q, e.g., $\mu_c = Qe^{-c}$. But this provokes the question of what is so special about the $\overline{\mathrm{MS}}$ scheme that in this scheme one should choose equality of μ and Q (a common choice in practice).

An answer is suggested by the method of renormalization subtraction of the asymptote given in Sec. 9.5. We found that $\mu_{\overline{\mathrm{MS}}}$ is like a cutoff at $k_{\mathrm{T}} = \mu_{\overline{\mathrm{MS}}}$, rather than some factor times this.

The method was applied to a coefficient function in (9.45), where there is a subtraction of the collinear region (e.g., by Fig. 9.3(c)), and then a renormalization of the UV divergence in the subtraction. After that there remains only a contribution from transverse momenta of some natural scale associated with Q, provided that z is not close to 0 or 1, and provided that μ is at this same scale. So the integral is of order unity, and is multiplied by the standard prefactor $g^2/4\pi^2$, and a group theory factor. This justifies the choice that $\mu_{\overline{\mathrm{MS}}}$ is within a modest factor of Q.

If instead we used the c scheme, then Sec. 9.5 shows that an appropriate choice would now be $\mu_c = Qe^{-c}$. Naturally, there is no need to require exactly one particular value of μ. The exact value of a structure function (or cross section) is independent of μ. Changing μ by a factor of 2 (for example) in a finite-order calculation of the hard scattering changes the numerical value of a computed structure function by an amount corresponding to the

expected truncation error of the perturbative calculation. Thus the effect of a modest change in μ is within the expected errors.

The simplest version of subtraction of the asymptote applies if there is no extra ϵ dependence in the integrand. If there is extra ϵ dependence, then it results in an extra finite term, as in the last line of (9.45). This can be regarded as being of a natural size for the quantity under consideration, so it does not affect arguments about large logarithms.

The idea that the cutoff should be of the natural size of the transverse momentum for a hard scattering (after subtraction of collinear and UV divergences) suggests that problems can occur when z is close to 0 or 1. This is visible in the logarithm of $(1 - z)/z$. An obvious choice of scale would then be $\mu^2 = Q^2(1 - z)/z$, corresponding to the range of the transverse-momentum integral.

However, in this case there are (at least) two very different physical scales in the hard scattering. Besides Q^2 there is the (square of) the photon-parton center-of-mass energy, $Q^2(1 - z)/z$. Even if we removed the large logarithm in this particular calculation, because it is dominated by the second scale, there would be other graphs with a natural scale Q. An example is the virtual vertex correction Fig. 9.4(d), in whose calculation the range of final-state energies is irrelevant. When different graphs need very different scales, a single choice of μ cannot eliminate all large logarithms. Instead improved factorization theorems are needed, for a genuinely fundamental solution of the problem.

When does this situation arise? Since $z = x/\xi$ and actual parton densities decrease with increasing ξ, one should not expect the case that z is small to be a concern. But when x gets large, the maximum $q\bar{q}$ mass is restricted: the kinematic limits on z are $x < z < 1$. This phenomenon is enhanced by the fact that typical parton densities fall rather rapidly with ξ above about a half, which disfavors the larger masses and keeps z close to unity.

This subject has been under active investigation, with improved factorization methods and resummation techniques being discovered. In any case the outcome is that when the typical value of z gets too close to unity, simple factorization is not an optimal technique.

9.9 NLO quark coefficient

To compute the NLO quark coefficient, we again use (9.35), but now with a quark target. The necessary graphs, including subtractions, are shown in Fig. 9.4. In all the calculations, we use (9.10) to replace the gluon polarization sum in the real-emission graphs by $-g^{\alpha\beta}$. Kinematics and normalization factors are the same as for the gluon-induced graphs (e.g., (9.36)) except for the replacement of the group theory factor T_F by C_F. We take the quark to be unpolarized, and perform the integral over azimuthal angles, using (A.36) and (A.37).

9.9.1 NLO quark coefficient for $\hat{F}_{\mathrm{L}j}$

The contribution to the longitudinal structure function is particularly simple. Because of the factors of l in the projection (9.2a) onto $\hat{F}_{\mathrm{L}j}$, graphs (b)–(e) all have a factor of $\not{l}$ next
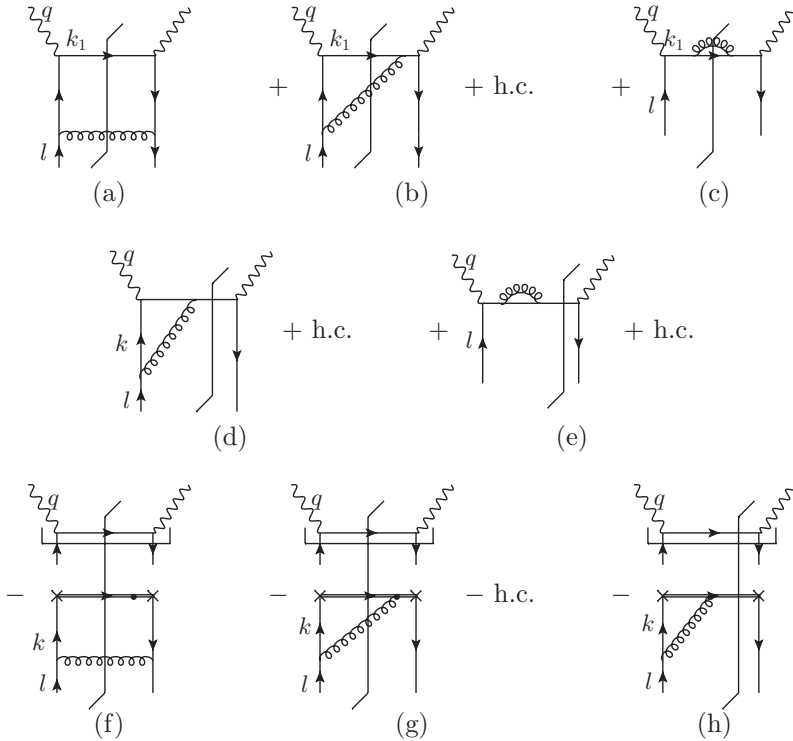
Fig. 9.4. Graphs for NLO quark coefficient function for DIS. Graphs with quark self-energies on the *incoming* quark line are not needed, since they cancel completely and exactly between the graphs for DIS on a quark target and the subtraction terms.

to the $\slashed{l}$ factor for the incoming quark. Thus all these graphs give zero: $(\slashed{l})^2 = l^2 = 0$. The subtraction graphs are also zero, because $\hat{F}_{\mathrm{L}j}$ vanishes in the parton model. All that remains is graph (a), which gives

$$
\begin{aligned}
\hat{F}_{\mathrm{L}j}((\mathrm{a})) = & -\frac{g^2 e_j^2 C_F}{64\pi^2} \left(\frac{16\pi\mu^2}{\hat{s}} \right)^{\epsilon} \frac{1}{\Gamma(1-\epsilon)} \int_{-1}^{1} \mathrm{d}\cos\theta \; (\sin\theta)^{-2\epsilon} \\
& \times \frac{8z^3}{Q^2} \frac{\tfrac{1}{2}\mathrm{Tr}\,\slashed{l}\gamma^{\alpha}(\slashed{l}-\slashed{k}_2)\slashed{l}\slashed{k}_1\slashed{l}(\slashed{l}-\slashed{k}_2)\gamma_{\alpha}}{[(l-k_2)^2]^2} \\
\overset{\epsilon\to 0}{=} & \frac{g^2 e_j^2 C_F z^2}{8\pi^2} \int_{-1}^{1} \mathrm{d}\cos\theta \; (1-\cos\theta).
\end{aligned}
\tag{9.46}
$$

This has no divergences, so the limit $\epsilon \to 0$ is safe, and we get

$$
\hat{F}_{\mathrm{L}j} = \frac{g^2 e_j^2 C_F z^2}{4\pi^2} + O(g^4).
\tag{9.47}
$$

9.9.2 Real-gluon graphs for $\hat{F}_{2j}$

We apply (9.2b) to the real-gluon graphs for $\hat{F}_{2j}$. For graph (a):

$$\hat{F}_{2j}(\text{a}) = \frac{g^2 e_j^2 C_F}{8\pi^2} \left(\frac{16\pi\mu^2}{\hat{s}}\right)^\epsilon \frac{1}{\Gamma(1-\epsilon)} \int_{-1}^{1} \mathrm{d}\cos\theta \ (\sin\theta)^{-2\epsilon}$$

$$\times \left\{ \frac{z(1-z)(1-\epsilon)}{1+\cos\theta} + 4(3-2\epsilon)z^2(1-\cos\theta) \right\}. \tag{9.48a}$$

The second part of the factor in braces arises from the $\hat{F}_L$ term in (9.2b). For graph (b), we have

$$\hat{F}_{2j}(\text{b} + \text{h.c.}) = \frac{g^2 e_j^2 C_F}{8\pi^2} \left(\frac{16\pi\mu^2}{\hat{s}}\right)^\epsilon \frac{z}{\Gamma(1-\epsilon)} \int_{-1}^{1} \mathrm{d}\cos\theta \ (\sin\theta)^{-2\epsilon}$$

$$\times \left\{ \frac{z}{1-z} \frac{1-\cos\theta}{1+\cos\theta} + \epsilon \right\}, \tag{9.48b}$$

where we include a factor 2 to allow for the hermitian conjugate graph. For graph (c)

$$\hat{F}_{2j}(\text{c}) = \frac{g^2 e_j^2 C_F}{8\pi^2} \left(\frac{16\pi\mu^2}{\hat{s}}\right)^\epsilon \frac{1}{\Gamma(1-\epsilon)} \int_{-1}^{1} \mathrm{d}\cos\theta \ (\sin\theta)^{-2\epsilon} \frac{z(1-\epsilon)}{1-z}(1+\cos\theta). \tag{9.48c}$$

Positions of the divergences

Graph (a) simply has a divergence at $\theta = \pi$, i.e., $\cos\theta = -1$. With the conventions by which the momentum k_2 is defined, this is where the gluon is collinear to the initial-state quark. Accordingly it will cancel against the same collinear divergence in the subtraction graph (f).

The other graphs have a more complicated pattern of divergences, involving soft gluons and gluons collinear to the outgoing quark, as is evidenced by the divergence in both graphs at $z \to 1$. Naturally, the divergence only fully manifests itself when we integrate over z. To analyze this quantitatively, we use the principles explained in Sec. 9.4.4, where we needed to treat parton densities as generalized functions. We now do the same for structure functions and the coefficient functions. The existence of the extra divergence(s) indicates, of course, that we will need to improve the proof of factorization. For the moment we just examine the phenomena.

Since both the extra kinds of divergence occur at $z = 1$, some care is needed to identify their kinematics correctly. The general nature of the divergences can be extracted, as always, from the Libby-Sterman analysis. For this analysis, it is convenient to boost to the Breit frame, where $q^+ = -Q/\sqrt{2}$, $q^- = Q/\sqrt{2}$, and $\boldsymbol{q}_\text{T} = \boldsymbol{0}_\text{T}$. Then:

- An initial-state collinear divergence is at $\theta \to \pi$ (i.e., $\cos\theta \to -1$) with z fixed and not equal to unity.
- A final-state collinear divergence is at $z \to 1$, with θ fixed and away from π. Each final-state particle is in the minus direction with momentum fractions $k_1^-/q^- = (1-\cos\theta)/2$

and $k_2^-/q^- = (1 + \cos\theta)/2$. Notice that the quark and gluon form an outgoing system, and that θ is the polar angle of each particle in the Breit frame.

- A soft-gluon divergence is at $\theta \to \pi$ *and* $z \to 1$.

It is misleadingly tempting to identify all of the $z \to 1$ divergences as soft.

Graph (b) has all three types of divergence, evidenced by its singularities at both $z \to 1$ and $\theta \to \pi$. But graph (a) has only an initial-state collinear divergence, and graph (c) only a final-state collinear divergence. As can be seen from (9.48), dimensional regularization with $\epsilon < 0$ regulates all the divergences.

After integral

We know that after we average over x (or z), the final-state lines become effectively off-shell. This will entail cancellation of final-state collinear and soft divergences between real and virtual graphs. The initial-state collinear divergences cancel against the subtraction graphs.

We could exhibit the cancellation at the level of the integrands. Instead we will evaluate the graphs separately, with dimensional regularization, and see the cancellations of the resulting poles at $\epsilon = 0$. The graphs give the following values, all multiplied by $g^2 e_j^2 C_F/(8\pi^2)$:

$$\text{(a):} \quad -\frac{z(1-z)}{\epsilon} + z(1-z)\left[T + \ln\frac{1-z}{z} + 1\right] + 3z^2, \tag{9.49a}$$

$$\text{(b):} \quad \frac{2}{\epsilon^2}\delta(z-1) + \frac{2}{\epsilon}\left[\delta(z-1)(-T+1) - \frac{z^2}{(1-z)_+}\right]$$

$$+ \delta(z-1)\left(T^2 - 2T + 4 - \frac{\pi^2}{2}\right) +$$

$$+ 2z^2\left[\frac{1}{(1-z)_+}(T-1) - \frac{\ln z}{1-z} + \left(\frac{\ln(1-z)}{1-z}\right)_+\right], \tag{9.49b}$$

$$\text{(c):} \quad -\frac{1}{2\epsilon}\delta(z-1) + \frac{1}{2}\delta(z-1)(T-1) + \frac{z}{2(1-z)_+}. \tag{9.49c}$$

where we have dropped terms of order ϵ and beyond, and we have defined

$$T = \ln\frac{Q^2}{\mu^2} + \gamma - \ln(4\pi). \tag{9.50}$$

The integrals over $\cos\theta$ were performed using (A.49). Then an expansion in powers of ϵ was made using (A.47), (A.48), and (A.54). We again see the appearance of plus distributions, which is very characteristic of QCD calculations.

The double pole in graph (b) is a result of the nesting between the soft and collinear divergences.

9.9.3 Virtual-gluon graphs for $\hat{F}_{2j}$

We already calculated the on-shell vertex subgraph used in Fig. 9.4(d); see Sec. 4.2.3. But now: (a) we have space-like instead of time-like q; (b) the trace with the external currents

is slightly different. We add to the graph a counterterm for its UV divergence, which is the lowest-order graph times $-[g^2 e_j^2 C_F/(16\pi^2)] S_\epsilon/\epsilon$, times a factor of 2 to allow for the hermitian conjugate graph. The result for graph (d) and its conjugate is

$$(\mathrm{d + h.c.}): \quad -\frac{2}{\epsilon^2}\delta(z-1) + \frac{2}{\epsilon}\delta(z-1)(T-2)$$

$$+ \delta(z-1)\left(-T^2 + 4T - \ln\frac{Q^2}{\mu^2} - 8 + \frac{\pi^2}{6}\right), \qquad (9.51)$$

again times $g^2 e_j^2 C_F/(8\pi^2)$. This has a double pole, a logarithm in the single pole, and a double logarithm in the ϵ-independent term, all due to the combination of soft and collinear divergences. All of these terms cancel against the corresponding terms for graph (b), which is the only graph related by moving the final-state cut.

Graph (e) just involves a self-energy times the lowest-order hard scattering. As we saw in $e^+ e^-$ total cross section, in Sec. 4.1, we apply the LSZ prescription. The dimensionally regulated massless self-energy gives a zero contribution. There remains the UV wave-function renormalization counterterm, which gives

$$(\mathrm{e + h.c.}): \quad \frac{S_\epsilon}{2\epsilon}\delta(z-1) = \frac{1}{2\epsilon}\delta(z-1) + \delta(z-1)\left(\ln(4\pi - \gamma) + O(\epsilon)\right). \qquad (9.52)$$

9.9.4 Subtraction graphs for $\hat{F}_{2j}$

The subtraction graphs (f)–(h) are simply a factor of $e_j^2 z$, for the parton-model coefficient function, times the one-loop quark-in-quark density, with the external self-energies omitted, all times a factor -1 because they are subtracted. As usual, the graphs themselves vanish in the massless limit, by the use of dimensional regularization. So we just need the UV counterterm, which is for $Z_2 Z_{jj}$, the factor Z_2 arising because we use the counterterm that allows the use of renormalized fields. With the same conventions as before we get

$$(\mathrm{f-h}): \quad \frac{S_\epsilon}{\epsilon}\left[\frac{z(1+z^2)}{(1-z)_+} + \frac{5}{2}\delta(z-1)\right]. \qquad (9.53)$$

9.9.5 Total

Adding the contributions of all the graphs and taking the $\epsilon \to 0$ limit gives the quark coefficient function. With the LO term, we have

$$\hat{F}_{2j}(Q^2, z; \alpha_s, \mu)$$

$$= e_j^2 \delta(z-1) + \frac{g^2 e_j^2 C_F}{16\pi^2} z\left[4\left(\frac{\ln(1-z)}{1-z}\right)_+ - 3\left(\frac{1}{1-z}\right)_+ - 2(1+z)\ln(1-z)\right.$$

$$\left. - 2\frac{1+z^2}{1-z}\ln z + 6 + 4z - \left(\frac{2\pi^2}{3} + 9\right)\delta(1-z)\right] + O(g^4). \qquad (9.54)$$

9.10 Hard scattering with quark masses

In the calculations so far, we have set quark masses to zero, and some of the methods relied on the property of dimensional regularization that scale-free integrals are zero. It is useful to see how to bring in non-zero quark masses. One purpose is to allow the effects of quark masses to be computed, although we will not give a detailed treatment of the effects of quark masses here. A second purpose is to show that calculations of hard-scattering coefficients are not tied to properties of the dimensional regularization scheme with massless particles.

A convenient method to allow for heavy quarks in the hard scattering is to always set to to zero the masses of external particles of the hard scattering, but to allow heavy particles to circulate inside the hard scattering (Collins, 1998a). We will not try to justify this prescription here.

We will restrict our attention to the simplest case of the gluon-induced NLO coefficient functions. The structure of the calculation is unchanged from that with massless quarks; i.e., we use (9.35) to determine the one-loop coefficient function, with a projection onto individual structure functions by (9.2). The actual graphs are Fig. 9.3, just as before.

Analytic calculations of one-loop graphs with masses are harder than with zero masses. We first quote the results for the unsubtracted graphs (a) and (b), which can be deduced from Aivazis *et al.* (1994). First for F_L:

$$\hat{F}_{\mathrm{L}g} = \sum_j \frac{g^2 e_j^2 T_F z}{4\pi^2} \theta(\hat{s} - 4m_j^2) \left\{ \frac{4Q^2 \Delta}{(Q^2 + \hat{s})^2} - L \frac{8m_j^2 Q^2}{(Q^2 + \hat{s})^2} \right\}, \qquad (9.55)$$

where

$$L = 2 \log \left[\frac{\sqrt{\hat{s}} + \sqrt{\hat{s} - 4m_j^2}}{2m_j} \right], \qquad (9.56)$$

$$\Delta = \sqrt{\hat{s}(\hat{s} - 4m_j^2)}, \qquad (9.57)$$

and $\hat{s} = Q^2(1 - z)/z$, as usual. There is a theta function implementing the quark-flavor-dependent threshold in $\hat{s}$. In the general factorization formulae, like (8.83), the threshold restricts ξ to the range $x(1 + 4m_j^2/Q^2) < \xi < 1$.

Note that there are some differences in conventions for defining structure functions in Aivazis *et al.* (1994), and that there appears to be a factor of T_F missing from their formulae. The result for $\hat{F}_{\mathrm{L}g}$ reduces to the previous one, (9.40), in the limit that the quark masses are zero.

As for F_2, we get

$$\hat{F}_{2g} = \sum_j \frac{g^2 e_j^2 T_F z}{4\pi^2} \left\{ \theta(\hat{s} - 4m_j^2) \left[L \frac{Q^4 + \hat{s}^2}{(Q^2 + \hat{s})^2} + \frac{[4Q^2\hat{s} - (\hat{s} - Q^2)^2]\Delta}{\hat{s}(Q^2 + \hat{s})^2} \right.\right.$$

$$\left.\left. + L \frac{4m_j^2(\hat{s} - 2Q^2 - 2m_j^2)}{(Q^2 + \hat{s})^2} - \frac{4m_j^2\Delta}{(Q^2 + \hat{s})^2} \right]\right.$$

$$\left. - [1 - 2z(1 - z)]\ln\frac{\mu^2}{m_j^2} \right\} + O(g^4), \tag{9.58}$$

where the logarithmic term in the last line is for the subtraction graph (c), calculated at (9.7), here multiplied by 2 to include both the quark and antiquark contributions. The remaining terms are for graphs (a) and (b), and were obtained from Aivazis *et al*. (1994). In the massless limit, the logarithmic divergences cancel, and the limit reproduces the previous calculation (9.43).

Observe the mismatch between the allowed ranges of z in the integrand. The term from graphs (a) and (b) obeys a threshold condition, but the subtraction term allows z to go up to unity, where $\hat{s} = 0$, i.e., to an unphysical value. The parton-model approximation applied to a quark line is responsible for the mismatch. The approximation changes final-state momenta, so that the approximated final state violates conservation of 4-momentum. The same violation is present in the integrand for the parton-model formula, i.e., the LO cross section.

Strictly speaking our formalism was derived for the inclusive cross section, integrated over hadronic final states, and the results correctly apply to that situation. But if one wishes to extend the formalism to observables more differential in the final state, the violation of momentum conservation can have important consequences. Genuinely solving this issue requires the avoidance of approximations on parton momenta when they are related to final-state momenta. As seen in recent work (Collins and Jung, 2005; Collins, Rogers, and Staśto 2008), one must rethink the whole formalism; new methods do not use parton densities, but more general quantities, parton correlation functions, which do not have the integral over k^- and k_T in their definition.

Note that the above calculation applies when the $\overline{\text{MS}}$ scheme is used. This is appropriate for quarks whose mass is at most of order Q. For heavier quarks, a change in scheme is appropriate. There are various ways proposed to do this. A method I prefer is a generalization of the CWZ scheme of Sec. 3.10 to deal with parton densities and factorization; this is the ACOT scheme of Aivazis *et al*. (1994), which is probably best used in a modified version as given in Kretzer *et al*. (2004); Krämer, Olness, and Soper (2000). See Thorne and Tung (2008) for a wider ranging review.

9.11 Critique of conventional treatments

Compared with our presentation so far, a very different approach to factorization is found in much of the literature (e.g., Dissertori, Knowles, and Schmelling, 2003; Ellis, Stirling, and

Webber, 1996). It involves a strong emphasis on the mass divergences in massless on-shell partonic reactions, and it asserts that factorization is a method of absorbing mass divergences into a redefinition of parton densities. In contrast, in our presentation the divergences were canceled by subtraction terms that were needed to avoid double counting between, for example, NLO contributions to hard-scattering coefficients and LO contributions.

In this section, we assess the other approach and see that it is physically misleading, if not actually wrong. As such, it is a profound obstacle to further progress in applying perturbative methods to more complicated situations in QCD. Luckily from a practical point of view, the two approaches give the same results for hard-scattering coefficients when parton masses are set to zero. Thus the physical errors do not propagate to numerical results in phenomenology, at least for the simplest reactions.

The approach can be traced back to certain of the early literature on factorization, notably Ellis *et al.* (1979) and Curci, Furmanski, and Petronzio (1980), and it can be summarized as follows:

1. *Assert* that the structure function (or cross section) under consideration is a convolution of a partonic structure function and parton densities:

$$W = \text{partonic struct fn.} \otimes \text{bare parton density}$$

$$= W^{\text{parton}} \otimes f^{\text{bare}}. \tag{9.59}$$

The convolution is defined in (8.81). In view of later steps in the presentation, the parton densities are called "bare parton densities".

2. All parton masses in the partonic structure function are set to zero. The parton(s) entering it from the parton density are set *on-shell* and massless, with zero transverse momentum.

3. There are IR/collinear divergences in the parton cross section. It was shown (Ellis *et al.*, 1979; Curci *et al.*, 1980) that the partonic cross sections are a convolution of a divergence factor and a finite cross section.

$$W^{\text{parton}} = C \otimes D. \tag{9.60}$$

4. The final factorization formula is obtained by use of the associativity of convolution to allow the divergences to be absorbed into a redefinition of the parton densities.

$$W = (C \otimes D) \otimes f^{\text{bare}} = C \otimes \left(D \otimes f^{\text{bare}} \right) = C \otimes f^{\text{ren}}, \tag{9.61}$$

where $f^{\text{ren}} = D \otimes f^{\text{bare}}$.

The final result is of the same form as the factorization formula in (8.81). Moreover, if the collinear divergences are quantified by poles in dimensional regularization, their removal is by the same formula as in our approach. This can be obtained from the remarks at the end of Sec. 9.7.4. The factorization of collinear divergences in massless parton scattering, (9.60), can in fact be obtained from factorization applied to a massless parton target, assisted by the observation that loop graphs for massless parton densities in partonic targets are exactly zero in dimensional regularization.

However, the identity of the results should not obscure the profound problems with the argument just presented.

The first problem is that the starting point, (9.59), is not given a proof. In Ellis *et al.* (1979) a reference is given to the classic book on the parton model by Feynman (1972), which very much predates knowledge of the complications caused by QCD. The bare parton densities are also not defined; they cannot coincide with any of the parton densities we have defined.

A serious physics issue is that the partonic structure function in (9.59) is exactly a structure function initiated by an on-shell parton with zero transverse momentum. For example, the first gluonic term has the form

$$\otimes \text{Bare gluon density} \qquad (9.62)$$

Here, the gluon is set on-shell, just as in our calculations in Sec. 9.7. There the justification was that there was a subtraction in the coefficient function and therefore it is dominated by wide-angle scattering. We could therefore neglect small components of l with respect to large components. But in (9.59) and (9.62) this is no longer justified, since there is no subtraction. Indeed a gluon confined inside a hadron is not exactly on-shell, and therefore the collinear divergence is cut off.

Similarly in a model theory where all the fields have mass, there are no true collinear divergences. An approximation in which partons are made massless in unsubtracted NLO graphs therefore introduces spurious divergences. In such a theory, parton densities defined by the standard operator formulae have no collinear divergences, before or after renormalization, so the idea of absorbing collinear divergences into a redefinition is not tenable.

Note carefully that there is terminological ambiguity between the two approaches. In our approach "bare parton density" refers to a parton density before renormalization; renormalization is then strictly an issue of eliminating UV divergences by a suitable redefinition, commonly with the $\overline{\text{MS}}$ scheme. In the other approach, "bare parton density" refers to the undefined quantities in (9.59). The renormalization-like procedure applied in (9.61) is a different procedure, even when the $\overline{\text{MS}}$ scheme is said to be used.

We conclude that it is entirely unphysical to describe the basis of factorization in terms of moving collinear divergences from partonic structure functions or cross sections into redefined parton densities. Naturally, attempting to extend an incorrect method to more general situations leads to a conceptual morass. It is more by luck than good physics that the same hard-scattering coefficients are obtained for standard reactions.

9.12 Summary of known higher-order corrections

Here I summarize the available information on the higher-order terms in the DGLAP kernels and the coefficient functions for DIS. They are both known to order α_s^3.

The non-singlet part of DGLAP kernels was calculated to this order by Moch, Vermaseren, and Vogt (2004), and the singlet part by Vogt, Moch, and Vermaseren (2004). The order α_s^2 kernel was found by Furmanski and Petronzio (1980). See also Hamberg and van Neerven (1992) for some issues concerning the gauge invariance of the calculation. We have already given the order α_s kernels in (9.6), (9.23), (9.24), and (9.25).

The DIS coefficient functions were calculated by Vermaseren, Vogt, and Moch (2005) to α_s^3. The order α_s^2 calculation was by Zijlstra and van Neerven (1992) and by Moch and Vermaseren (2000). We have already given the order α_s coefficients in (9.40), (9.43), (9.47), and (9.54), with the parton model (α_s^0) at (9.1).

It is also worth mentioning the results at order α_s^2 for the Drell-Yan process, in Anastasiou *et al.* (2003, 2004), which are relevant to the same kind of precision phenomenology.

9.13 Phenomenology

Much of the predictive power of QCD is from factorization properties, both for inclusive DIS and for many other reactions. The equations used are for factorization of structure functions and cross sections, and for DGLAP evolution:

$$\sigma = \hat{\sigma} \otimes f, \quad \sigma = f_1 \otimes \hat{\sigma} \otimes f_2, \tag{9.63}$$

$$\frac{\mathrm{d} f}{\mathrm{d} \ln \mu} = 2P \otimes f. \tag{9.64}$$

Here σ is a measurable cross section or structure function, $\hat{\sigma}$ is a corresponding hard-scattering coefficient, while f, f_1 and f_2 are parton densities. Factorization is accurate up to power-law corrections in a hard scale Q. The second form of factorization applies to hard reactions in hadron-hadron collisions, where there is a parton density in each hadron.

The hard-scattering coefficients and the DGLAP kernel P are perturbative calculable in powers of the small coupling $\alpha_s(Q)$, and so we regard them as approximately calculable from first principles. The non-perturbative information is contained in the parton densities at some chosen fixed large scale, since the evolution to other large scales is perturbatively controlled. However, at present there is little ability to estimate or model the non-perturbative parton densities from first principles.

The predictive power lies in the universality of the parton densities. Parton densities are the same in all reactions, and, apart from the perturbative DGLAP evolution, they are the same at all values of Q. Thus essentially the following scheme works:

- Fit parton densities for some value of the scale μ from data on a limited set of experiments at one energy, using perturbatively calculated hard-scattering coefficients and DGLAP kernels.
- Evolve the parton densities to other scales.
- Predict cross sections at other energies and for other reactions.

In reality, data is of limited precision, and data on each individual reaction is only useful in determining some particular flavor combinations of parton densities. Therefore global
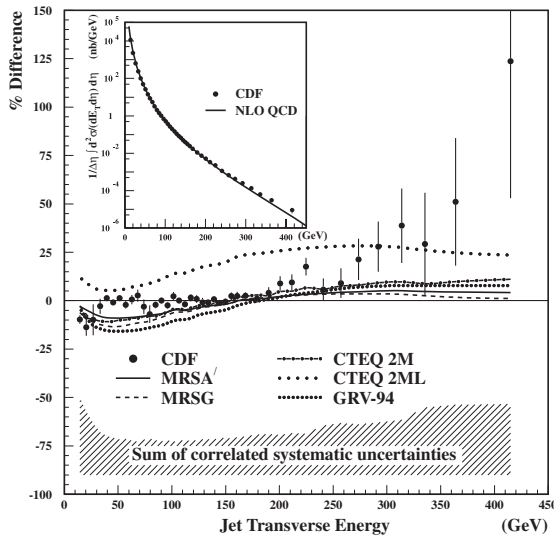
Fig. 9.5. Jet cross section and QCD *predictions* at CDF experiment (Abe *et al*., 1996). The figure is copyright (1996) by The American Physical Society, and reproduced by courtesy of the CDF collaboration.

analyses are made to a wide variety of data, chosen for situations where the likely errors on both theory and experiment are judged to be sufficiently small. Thus the global analyses simultaneously fit parton densities and test QCD through measures of the goodness of fit. The amount of data is large, so this is a non-trivial undertaking.

Currently the main global analyses are:

- by the members of the CTEQ collaboration (Tung *et al*., 2007);
- by a group in the UK going under the acronyms MRST and recently MSTW (Martin *et al*., 2007);
- by Alekhin and collaborators (Alekhin, Melnikov, and Petriello, 2006).

In addition, the two *ep* collider experiments at DESY have made fits to their own data: ZEUS (Chekanov *et al*., 2005) and H1 (Adloff *et al*., 2003). They have taken advantage of the availability of charged-current processes to gain flavor separation of the parton densities.

Another group (Del Debbio *et al*., 2007) is working towards a global fit using rather different calculational technique based on neural-network methods.

An example of the predictive power is shown in Fig. 9.5. Here a measurement (Abe *et al*., 1996) by the CDF collaboration is shown for the production of jets of high transverse energy, E_{T}, in proton-antiproton collisions, and it is compared with QCD predictions. Although this is now a rather old comparison, its importance is that there is a genuine prediction. Parton densities at that period were measured in other processes and the perturbative hard-scattering calculations are, of course, from QCD first principles.

The agreement is good, except possibly at the largest values of E_T, but even there not outside the rather large errors. Since then it has been realized that this reaction is a most sensitive one for measuring the gluon density at large parton ξ. Therefore later work has frequently used jet data from hadron-hadron collisions in making global fits for parton densities. Thus the QCD calculations presented with the latest data can no longer be considered pure predictions. Results are available from both CDF (Abulencia *et al.*, 2007) and D0 (Abazov *et al.*, 2008) collaborations.

There are many other processes where QCD predictions have been made, by and large with success.

Exercises

9.1 Finish the calculations of the one-loop renormalization of parton densities by doing the calculations for gluon-in-quark and gluon-in-gluon, thereby verifying (9.24) and (9.25).

9.2 Verify the sum rules (8.41) and (8.42) for quark number and for momentum at one-loop order.

9.3 Verify the results in Sec. 9.5.2.

9.4 Find the gluon-induced NLO correction in a version of QCD where quarks are scalars.

9.5 (***) Using pdfs from some standard fit, obtain some estimates of the typical value of z in integrals of parton densities and hard scattering like those in (9.43), etc. You can probably do this by obtaining diagnostics from a numerical quadrature, although it should also be possible to obtain some order-of-magnitude results more analytically. Draw some conclusions about the reliability of standard perturbative QCD calculations under various kinematic conditions.

9.6 Consider the graph of Fig. 9.3(a) for the photon-gluon process, and suppose that the quarks are given a mass m_q. Show that the minimum fractional plus momentum of the intermediate quark line is $\chi = x(1 + 4m_q^2/Q^2)$. Fractional plus momentum of the intermediate quark means $(k_1^+ - q^+)/P^+$. [See the definition given in Tung, Kretzer, and Schmidt (2002) for the ACOT(χ) scheme for treating heavy quarks in factorization.]

9.7 Generalize the result of problem 9.6 to the case that the current is flavor changing between quarks of different masses, m_1 and m_2.

9.8 Verify the calculations giving the NLO quark contribution to F_2, i.e., (9.48).